ISSN 0915-633X

NATIONAL INSTITUTE FOR FUSION SCIENCE

Symmetry Breaking by Differential Rotation and Saddle-node Bifurcation of the Thermal Convection in a Spherical Shell

K. Araki, S. Yanase and J. Mizushima

(Received - Nov. 17, 1995)

NIFS-387 Dec. 1995

RESEARCH REPORT
NIFS Series

NAGOYA, JAPAN

Symmetry breaking by differential rotation and saddle-node bifurcation of the thermal convection in a spherical shell

Keisuke Araki, Shinichiro Yanase*,and Jiro Mizushima**

Theory and Computer Simulation Center,
National Institute for Fusion Science, Nagoya 464-01, Japan
*Engineering Mathematics, Faculty of Engineering,
Okayama University, Okayama 700, Japan
**Department of Mechanical Engineering, Faculty of Engineering,
Doshisha University, Kyoto 610-03 Japan

Abstract The effect of a weak azimuthal shear flow on the Bénard convection in a spherical shell is investigated numerically where gravity is directed to the center of the spheres. Differential rotation of the spheres is introduced as the simplest driving mechanism of the shear flow. Axisymmetric steady solutions are obtained by an iterative method and their stability is analyzed. Bifurcation diagram of the steady solutions is extensively searched over the parameter space. It is shown by both the fully numerical calculation and the weakly nonlinear analysis that the weak shear flow breaks the asymptotic reflection symmetry due to the self-adjointness of the linearized system so that the pitchfork bifurcation is deformed and the saddle-node bifurcation occurs.

Keywords: thermal convection, spherical shell, saddle-node bifurcation, symmetry breaking by differential rotation.

1 Introduction

Thermal convection in a spherical shell has attracted many researchers because of its typical geometry in geophysics and astrophysics. The early studies of linear stability are reviewed in the monograph by Chandrasekhar.[1] The system has the spherical symmetry which causes the degeneracy of the linear solutions. The $\mathbf{O}(3)$ symmetry breaking bifurcation and the consequent pattern selection have been investigated by many authors since Busse initiated [2]. The bifurcation problem is now intensively investigated in terms of the equivariant unfolding theory [3] and bifurcation diagrams for steady solutions are obtained in detail for a single mode interaction case [4] and for 2-modes interactions case [5].

The effect of rotation on the thermal convection within a spherical shell has been one of the most important themes in the study of dynamics inside celestial bodies. Among the models which take rotation effects into account, two typical models exist. One is the solid-body rotation model where the whole system rotates at a constant angular velocity. In this system the Coriolis force plays an important roll and most researches have been devoted to the study of the effect of a solid-body rotation on the thermal convection. The other is the differential rotation model where two spheres rotates at different angular velocities. This is probably the simplest model which includes the effect of shear flow in the azimuthal direction on the thermal convection.

The azimuthal shear flow in a spherical shell without thermal effects yields the flow in the meridional direction by nonlinear interactions. This flow is known as the spherical Taylor-Couette flow and has been studied from the engineering viewpoint [6, 7, 8]. The instability of the basic solution which causes the secondary Taylor vortices is experimentally found to occur only for $R > 4.35$, where R is the ratio of the inner sphere radius to the gap width[9]. The bifurcations of axisymmetric solutions has been studied numerically by Mamum and Tuckerman[10].

There exist few works treating the effect of azimuthal shear flows on the thermal convection in a spherical shell in spite of its importance in geophysics and astrophysics. Araki, Yanase and Mizushima studied the effect of the differential rotation on the thermal convection in a spherical shell[11, 12]. The axisymmetric steady solutions are obtained numerically for the cases with and without rotation. The coexistence of the pitchfork bifurcation and the imperfect pitchfork, i.e., saddle-node bifurcation is found[12].

From the point of view of bifurcation theory, the existence of rotation, whether it is solid-body or differential, is interesting because it breaks the spherical symmetry of the system so that the spherical symmetry is reduced to the axisymmetry. This effect results in removing the degeneracy of the linear stability problem with the spherical symmetry and changes the feature of the bifurcation. As for the symmetry of the system, there are two types of bifurcation for the convection in a spherical shell with rotation. One is the bifurcation which breaks $\mathbf{O}(2)$ symmetry and the other is the bifurcation which retains $\mathbf{O}(2)$ symmetry.

It is well known that, in the solid-body rotation case, the most unstable disturbance is a non-axisymmetric mode which is given by a sectoral harmonic and the bifurcation is generically a Hopf type.

In our previous work we treated the problem with the differential rotation with $\mathbf{O}(2)$ symmetry and in the present work, we still concentrate on the case with $\mathbf{O}(2)$ symmetry. The reason why we treat only the axisymmetric solutions is as follows: 1. In order to investigate the full non-axisymmetric problem, the axisymmetric solutions are the basis and the solutions are very diverse even if they are assumed to be axisymmetric. Thus we must investigate the bifurcations of the axisymmetric solutions at least as the first step to the full non-axisymmetric problem. 2. Under the effect of the azimuthal shear, it is plausible that the axisymmetric convection is the most unstable judging from the result of the Rayleigh-Bénard convection

with a plane shear[13].

For the bifurcation study, we utilize the Newton-Raphson's iteration method to obtain the nonlinear steady solutions. The time marching method is not appropriate for the present purpose to obtain steady solutions because they exclude unstable solutions, and it is often observed that some unsteady solutions stay around an unstable steady state for an extremely long time. We also investigate the linear stability of the nonlinear steady solutions against axisymmetric disturbances.

In §2, the basic equations and the numerical method are given. The section 3 is dedicated to the presentation of the numerical results. The symmetry of the system and the symmetry breaking by a weak shear flow is analyzed in §4. Summary and discussions are given in §5.

2 Basic equations

Consider a fluid layer between two concentric spheres as sketched in Fig.1. The radii of the inner and outer spheres are r_1 and $r_1 + d$ respectively. The gravity acceleration is directed to the center of the spheres and its amplitude is proportional to r^{-2}. The inner sphere rotates at an angular velocity Ω, and the outer one is fixed. The temperature of the inner sphere is kept to be $T_0 + \Delta T$ and that of the outer one is T_0. The spherical coordinates (r, ϑ, φ) are introduced.

The perfectly conducting boundary condition is adopted for the temperature and the rigid boundary condition for the velocity. Then, the boundary conditions are

$$\mathbf{u} = r_1\Omega \sin\vartheta \mathbf{e}_\varphi, \quad T = T_0 + \Delta T \quad \text{at } r = r_1, \tag{1a}$$

$$\mathbf{u} = \mathbf{0}, \qquad T = T_0 \qquad \text{at } r = r_1 + d, \tag{1b}$$

where $\mathbf{e}_\varphi$ is the unit vector in the φ direction.

The variables are nondimensionalized by using the gap width d, the thermal

diffusivity κ and the temperature difference ΔT. Then, the present system has four dimensionless parameters: the aspect ratio $R = r_1/d$, the Rayleigh number $Ra = \alpha g_0 \Delta T d^3/\kappa\nu$, the Reynolds number $Re = r_1^2\Omega/\nu$ and the Prandtl number $Pr = \nu/\kappa$, where α is the coefficient of thermal expansion and g_0 is the gravity acceleration on the inner sphere.

In this paper we assume that the flow is axisymmetric with respect to the rotation axis. Under this assumption, the incompressible velocity field $\mathbf{u}$ is expressed in terms of the meridional stream function Ψ and the azimuthal stream function ω as

$$u_r = \frac{1}{r^2 \sin\vartheta}\frac{\partial \Psi}{\partial \vartheta}, \quad u_\vartheta = -\frac{1}{r\sin\vartheta}\frac{\partial \Psi}{\partial r}, \quad u_\varphi = \frac{\omega}{r\sin\vartheta}. \tag{2}$$

Under the Boussinesq approximation, the equation of motion and the equation of thermal conduction for Ψ, ω and T are given as follows:

$$\frac{\partial D^2\Psi}{\partial t} = N_1(\omega,\ \omega) + N_2(\Psi,\ \Psi) + PrRa\left(\frac{R^2}{r^2}\right)\frac{\partial T}{\partial \vartheta}\sin\vartheta + PrD^2D^2\Psi, \tag{3a}$$

$$\frac{\partial \omega}{\partial t} = J(\Psi,\ \omega) + PrD^2\omega, \tag{3b}$$

$$\frac{\partial T}{\partial t} = J(\Psi,\ T) + \Delta T, \tag{3c}$$

where J, N_1, N_2, D^2 and Δ are operators defined by

$$J(f,\ g) = \frac{1}{r^2\sin\vartheta}\left(\frac{\partial f}{\partial r}\frac{\partial g}{\partial \vartheta} - \frac{\partial f}{\partial \vartheta}\frac{\partial g}{\partial r}\right), \tag{4a}$$

$$N_1(f,\ g) = -\frac{2f}{r^2\sin^2\vartheta}\left(\frac{\partial g}{\partial r}\cos\vartheta - \frac{\partial g}{\partial \vartheta}\frac{\sin\vartheta}{r}\right), \tag{4b}$$

$$N_2(f,\ g) = J(f,\ D^2g) + N_1(D^2f,\ g), \tag{4c}$$

$$D^2 = \frac{\partial^2}{\partial r^2} + \frac{\sin\vartheta}{r^2}\frac{\partial}{\partial \vartheta}\frac{1}{\sin\vartheta}\frac{\partial}{\partial \vartheta}, \tag{4d}$$

$$\Delta = \frac{1}{r^2}\frac{\partial}{\partial r}r^2\frac{\partial}{\partial r} + \frac{1}{r^2\sin\vartheta}\frac{\partial}{\partial \vartheta}\sin\vartheta\frac{\partial}{\partial \vartheta}. \tag{4e}$$

We calculate the steady solutions of Eqs.(3a)-(3c) numerically by using the collocation method together with the Newton-Raphson's iteration method. The linear

stability analysis of the obtained steady solutions is carried out by the collocation method with the double QR algorithm.

For the sake of convenience for numerical calculation of the steady solutions, ω and T are divided into two parts as follows:

$$\omega(r,\vartheta) = \omega_{st}(r,\vartheta) + \hat{\omega}(r,\vartheta), \tag{5a}$$

$$T(r,\vartheta) = T_{eq}(r) + \hat{T}(r,\vartheta), \tag{5b}$$

where ω_{st} is the Stokes solution and T_{eq} is the conductive solution. The Stokes solution ω_{st} which satisfies $D^2\omega_{st} = 0$ and the boundary conditions (1a) and (1b) is given by

$$\omega_{st}(r,\ \vartheta) = \frac{RePrR\sin^2\vartheta}{(R+1)^3 - R^3}\left[\frac{(R+1)^3}{r} - r^2\right]. \tag{6}$$

The conductive solution T_{eq} which satisfies the equation $\Delta T_{eq} = 0$ and the boundary conditions (1a) and (1b) is given by

$$T_{eq}(r) = \frac{T_0}{\Delta T} + R\left(\frac{R+1}{r} - 1\right). \tag{7}$$

The dependent variables $\Psi(r,\vartheta)$, $\hat{\omega}(r,\vartheta)$ and $\hat{T}(r,\vartheta)$ are expanded as

$$\Psi(r,\vartheta) = \sum_{m=0}^{M}\sum_{l=1}^{N+1}\Psi_{ml}(1-x^2)^2T_m(x)\tilde{P}_l(\cos\vartheta), \tag{8a}$$

$$\hat{\omega}(r,\vartheta) = \sum_{m=0}^{M}\sum_{l=1}^{N+1}\hat{\omega}_{ml}(1-x^2)T_m(x)\tilde{P}_l(\cos\vartheta), \tag{8b}$$

$$\hat{T}(r,\vartheta) = \sum_{m=0}^{M}\sum_{l=0}^{N}\hat{T}_{ml}(1-x^2)T_m(x)P_l(\cos\vartheta), \tag{8c}$$

where $T_m(x)$ is the m-th order Chebyshev polynomial and $x = 2(r-R)-1$. The function $P_l(\cos\vartheta)$ is the l-th order Legendre polynomial and $\tilde{P}_l(\cos\vartheta)$ is defined by

$$\tilde{P}_l(\cos\vartheta) = \sin\vartheta\frac{\partial}{\partial\vartheta}P_l(\cos\vartheta) = \sin\vartheta P_l^1(\cos\vartheta). \tag{9}$$

For the linear stability analysis of the steady solution, the disturbances for Ψ, ω and T are expanded in the same way as Eqs.(8a)-(8c) for the spatial variables

and the time dependence of the disturbances is assumed to be $\exp(\sigma t)$ where σ is a complex number.

3 Results of numerical calculation

Time independent solutions Eqs.(3a)-(3c) are obtained and their linear stability against the axisymmetric disturbances are analyzed in the parameter range of $2500 < Ra < 3000$ and $0 < Re < 70$ for the aspect ratio $R = 2.23$. The Prandtl number Pr is fixed to 7. In the following we call the solution symmetric with respect to te equator as the *symmetric solution* and the solution which has no symmetry with respect to the equator is called as the *asymmetric solution*. We have studied the bifurcation of the *asymmetric* solution and the effect of the differential rotation has been treated in Ref.[12]. In the present paper we concentrate the study of the bifurcations of the *symmetric* solutions.

In the numerical calculation, the truncation numbers M and N in the r- and ϑ-directions were taken to be 8 and 64 respectively. To obtain the symmetric solutions we take 32 modes with even l's in the ϑ-direction considering the equatorial symmetry. The linear stability analysis of the obtained solutions is, on the other hand, carried out for both the symmetric and antisymmetric disturbances. We assured the numerical accuracy by observing that the Nusselt number defined below does not change in five significant digits with doubling the truncation numbers M and N.

When the differential rotation is absent, the most unstable disturbance of the linear stability of the fluid at rest is given by the *symmetric* mode of $l = 8$ in the range of $2.10 < R < 2.40$[14]. (Remember that the system has the spherical symmetry for $Re = 0$ so that each eigenfunction of the linear stability problem must be expressed by a Legendre function $P_l(\cos\vartheta)$ with a fixed l.) In the case of the aspect ratio $R = 2.23$ the critical Rayleigh number Ra_c is 2541.7. At

this aspect ratio, the difference between the critical Rayleigh number Ra_c and the second eigenvalue Ra (for $l = 7$ or 9, antisymmetric) is the largest so that the most unstable mode is thought to be least influenced by other modes. This is the reason why we take the value $R = 2.23$ in the present work.

We adopt two quantities characterizing the nonlinear steady state: the ratio of convective heat transfer to conductive heat transfer $Nu - 1$ where Nu is the Nusselt number and the radial velocity at the equator $u_0 \equiv u_r(R + 1/2, \pi/2)$. The Nusselt number is defined by

$$Nu = \frac{\iint \frac{\partial T}{\partial r} \sin\vartheta \mathrm{d}\vartheta \mathrm{d}\varphi}{\iint \frac{\mathrm{d}T_{eq}}{\mathrm{d}r} \sin\vartheta \mathrm{d}\vartheta \mathrm{d}\varphi} = 1 - \frac{4(R+1)}{R} \sum_{m=0}^{M} \hat{T}_{m0}, \tag{10}$$

where the integration is carried out on the outer sphere $r = R + 1$.

First we consider the case without the differential rotation ($Re = 0$) over the range $Ra \leq 3000$. For $R = 2.23$, the most unstable mode is symmetric with $l = 8$ and the critical Rayleigh number $Ra_c = 2541.7$. Up to $Ra = 3000$, there are the second and the third symmetric unstable modes which correspond to $l = 10$ and $l = 6$ and their critical Rayleigh numbers are 2732.0 and 2786.5 respectively. The values of u_0 and $Nu - 1$ of the solutions bifurcated from these unstable modes are plotted for $Re = 0$ in Figs.2(a) and (b) respectively. The contours of $\Psi(r, \vartheta)$ for these solutions are also depicted for $Ra = 3000$ in Fig.2(b).

The bifurcation diagram for u_0 in Fig.2(a) shows that the bifurcations are the supercritical pitchfork ones. The absolute value of u_0 of the upward solution ($u_0 > 0$) is slightly larger than that of the downward solution ($u_0 < 0$) for an assigned Ra and the difference grows as Ra increases. In the following, we name each branch after the direction of flow at the equator and the number of convection rolls in the solution. For example the name of the branch denoted by open circles is the *upward 8-roll* solution.

The symbols used in the Fig.2(b) are the same as those in Fig.2(a). The

Nusselt numbers are nearly proportional to $Ra - Ra_c$ for both the upward and the downward 8-roll branches. This result implies that the amplitude equation of the bifurcation is well approximated by the cubic Landau equation.

The linear stability analysis of the steady solutions shows that both the 8-roll solutions are stable to axisymmetric disturbances and all the other solutions are unstable to axisymmetric disturbances.

Next we consider the case with the differential rotation. In the present work, we investigate the range over $Re \leq 70$ and $Ra \leq 3000$. For this parameter range of the Reynolds number, the centrifugal instability of the spherical Taylor-Couette flow may not occur. It should be remarked that, when the differential rotation is exerted, a steady circulating solution appears and the trivial (motionless) solution no longer exists.

The values of u_0 and $Nu-1$ of the solutions are plotted for $Re = 20$ in Figs.3(a) and (b) respectively. These figures show that pitchfork bifurcations which occur for $Re = 0$ become imperfect for $Re > 0$. The bifurcation branches split as follows: (I) the smooth transition from the 2-roll solution to the upward 8-roll solution, (II) saddle-node bifurcation to the downward 8-roll solution and the 2-roll solution that is smoothly connected to the downward 10-roll solution, (III) saddle-node bifurcation to the upward 10-roll solution and the 2-roll solution that is smoothly connected to the upward 6-roll solution and (IV) saddle-node bifurcation to the downward 6-roll solution and the 2-roll solution. The symbols on the branches in Figs.3(a) and (b) are chosen considering the topological continuity with those in Figs.2(a) and (b). For example, the branch with open circles in Figs.3(a) and (b) (the branch (I)) are obtained from the branch with the same symbols in Figs.2(a) and (b) (the upward 8-roll solution) by changing the Reynolds and the Rayleigh numbers adiabatically.

It is remarkable that the deformation to the saddle-node bifurcation occurs

at all the symmetric solution branches. These deformations are regarded as the result of the symmetry breaking by the weak shear flow induced by the differential rotation of the boundaries. What kind of symmetry of the system is relevant and how this symmetry is broken? We discuss this symmetry breaking in the next section.

The Nusselt number of the 8-roll solutions in Fig.3(b) shows the almost linear dependence on the Rayleigh number. In the same figure, the meridional stream functions for $Re = 20$ and $Ra = 3000$ are also depicted.

The linear stability analysis of the steady solutions shows that the solution on the branch (I) and the 8-roll part of the branch (II) are stable to axisymmetric disturbances and all the other solutions are unstable to axisymmetric disturbances.

4 Symmetry of the solution

It was numerically assured that all the symmetric solutions experience the pitchfork bifurcation when differential rotation is absent ($Re = 0$) and that these pitchfork bifurcations become imperfect for the case of $Re > 0$. These facts imply that the reflection symmetry which exists in the system for $Re = 0$ is broken by the differential rotation. In our previous work[12] the bifurcation of both symmetric and asymmetric solutions were investigated numerically and it was shown that asymmetric solution branches appear via a pitchfork bifurcation even when the differential rotation is exerted. What makes the difference between the symmetric solution case and the asymmetric one? What kind of symmetry is relevant to the pitchfork bifurcation of the symmetric solution? In this section we will analyze the symmetry which the system intrinsically has and the mechanism of the symmetry breaking which causes the deformation of the pitchfork bifurcation into the saddle-node bifurcation.

4.1 equatorial symmetry (Z_2 symmetry) of the system and pitchfork bifurcation of asymmetric solution

We write the basic equations (3a)-(3c) symbolically as

$$\frac{\partial \mathbf{X}}{\partial t} = \mathbf{F}(\mathbf{X}), \tag{11}$$

$$\mathbf{X} = (\Psi(r,\vartheta,t), \omega(r,\vartheta,t), T(r,\vartheta,t)). \tag{12}$$

The system has a reflectional symmetry with respect to $\vartheta = \pi/2$, i.e., $\mathbf{Z}_2$ symmetry. In the following we call this symmetry the *equatorial* symmetry. Let Γ be a equatorial reflection operator, which acts on $\mathbf{X}$ as

$$\Gamma\left(\Psi(\vartheta),\ \omega(\vartheta),\ T(\vartheta)\right) = \left(-\Psi(\pi-\vartheta),\ \omega(\pi-\vartheta),\ T(\pi-\vartheta)\right). \tag{13}$$

It is easy to verify that $\mathbf{F}$ is $\mathbf{Z}_2$ equivariant,

$$\Gamma(\mathbf{F}(\mathbf{X})) = \mathbf{F}(\Gamma(\mathbf{X})), \tag{14}$$

even for the case with the differential rotation.

Let H be the function space of the solutions of Eqs.(3a)-(3c). Since $\Gamma^2 = id$, where id denotes the identity operator, the eigenvalues of Γ are ± 1. Thus H is decomposed into two subspaces according to these eigenvalues. We denote the subspace that corresponds to eigenvalue 1 by H_S and that to eigenvalue -1 by H_A. According to this decomposition, any solution $\mathbf{X}$ can be decomposed into *symmetric* components $\mathbf{X}_S$ and *antisymmetric* components $\mathbf{X}_A$ as follows:

$$\mathbf{X} = \mathbf{X}_S + \mathbf{X}_A \tag{15}$$

where

$$\mathbf{X}_S = \frac{1}{2}(\mathbf{X} + \Gamma\mathbf{X}) \in H_S, \qquad \mathbf{X}_A = \frac{1}{2}(\mathbf{X} - \Gamma\mathbf{X}) \in H_A. \tag{16}$$

Because the nonlinear interactions between antisymmetric components yield symmetric components, no antisymmetric solution exists. Therefore the system

allows symmetric solutions $\mathbf{X} = \mathbf{X}_S$ and asymmetric solutions $\mathbf{X} = \mathbf{X}_S + \mathbf{X}_A$. It should be remarked that all the symmetric solutions are the fixed points of the operator Γ.

Now we discuss the qualitative character of the bifurcation from the trivial (motionless) solution $\mathbf{X} = \mathbf{0}$ for $Re = 0$ and from the steady symmetric solution $\mathbf{X} = \mathbf{X}_S$ for $Re > 0$, which occurs as the Rayleigh number Ra increases. For these steady solutions, the unstable disturbance at the critical point is antisymmetric or symmetric. Our purpose is to make it clear that the characters of the bifurcation differ according to whether the unstable disturbance is antisymmetric or symmetric.

When an antisymmetric disturbance becomes unstable, the bifurcated solution is asymmetric. In this case one may understand that the equatorial symmetry guarantees the pitchfork bifurcation whether the differential rotation exists or not in the following manner (see Fig.4). Suppose that an asymmetric solution branch $\mathbf{X}_1 = \mathbf{X}_{S1} + \mathbf{X}_{A1}$ bifurcates from a steady symmetric solution $\mathbf{X}_{S0}$ after an antisymmetric disturbance is destabilized. Due to the equatorial symmetry, one can obtain another branch $\mathbf{X}_2$ by operating Γ on the branch, i.e., $\mathbf{X}_2 = \Gamma(\mathbf{X}_1) = \mathbf{X}_{S1} - \mathbf{X}_{A1}$. The branch $\mathbf{X}_2$ also stems from the solution $\mathbf{X}_{S0}$. As the solutions $\mathbf{X}_1$ and $\mathbf{X}_2$ approach the bifurcation point, the antisymmetric component $\mathbf{X}_{A1}$ tends to zero and the two branches coincide at the point. Thus one can obtain the bifurcation diagram of pitchfork type. Therefore these two solutions on the bifurcation branches have exactly the same physical properties such as the Nusselt number for assigned Ra, Re and R.

4.2 self-adjointness of the linearized system, the pitchfork bifurcation of symmetric solution and symmetry breaking by a weak shear flow

The equatorial symmetry discussed in the previous subsection is not relevant to the pitchfork bifurcation of the *symmetric* solutions. The discussion given above made use of the reversal of the antisymmetric components $\mathbf{X}_A$ by the operation of Γ. All the symmetric solutions $\mathbf{X}_S$, on the other hand, are the fixed points of Γ: $\Gamma(\mathbf{X}_S) = \mathbf{X}_S$. Thus in the equatorial symmetry we cannot find any mechanisms that guarantee the reversal of a solution from one branch to the other.

For the symmetric solution case, the reflection symmetry is a consequence of the self-adjointness of the linearized system. It can be demonstrated by use of the weakly nonlinear perturbation analysis, the details of which is presented in the Appendix. Following the perturbation analysis, it is shown that the self-adjointness of the linearized system inhibits the appearance of the quadratic term and that the nonlinear term of the normal form must begin with the cubic term. At $O(\epsilon^3)$, we obtain the amplitude equation for $Re = 0$,

$$\frac{\mathrm{d}A}{\mathrm{d}t} = (Ra - Ra_c)\lambda_0 A + \lambda_1 A^3, \tag{17}$$

where $\epsilon = \sqrt{Ra - Ra_c}$ and A is a real variable which represents the amplitude of the convection and depends on the time t, and λ_0, λ_1 are constants given by the solvability conditions. Thus the bifurcation is a pitchfork so that the resulting amplitude equation possesses an asymptotic reflectional symmetry with respect to the change of the sign of A. The term 'asymptotic' is used here because in the non-perturbative system, the rigorous symmetry holds only asymptotically around the bifurcation point. The numerical result that the Nusselt number is almost a linear function of $(Ra - Ra_c)$ implies that the dynamics of the system is well approximated by this amplitude equation and that the perturbation analysis upto this order is adequate for discussing the symmetry of the system qualitatively.

How does, then, the differential rotation break this symmetry? We observed that the pitchfork bifurcation branches break into two parts, two branches from a saddle-node bifurcation point and a smoothly extended branch. This type of bifurcation diagram generically occurs when a constant term is added in the normal form (17).

When the differential rotation exists, the significant feature of the basic equations (3a)-(3c) is that azimuthal flow ω is not zero so that the azimuthal flow term $N_1(\omega,\omega)$ in the equation (3a) does not vanish. Thus the amplitude equation (17) is modified into

$$\frac{\mathrm{d}A}{\mathrm{d}t} = (Ra - Ra_c)\lambda_0 A + \lambda_1 A^3 + \lambda_2, \tag{18}$$

where λ_2 is given by

$$\lambda_2 = \frac{\left\langle \tilde{\mathbf{X}}^{\dagger}, (N_1(\omega,\omega),0)\right\rangle}{\left\langle \tilde{\mathbf{X}}, M\tilde{\mathbf{X}}\right\rangle} \tag{19}$$

(about notations see Eqs.(4) and the Appendix). Eq.(18) and (19) constitute the normal form of the present problem. Because the equation of ω couples with Ψ, λ_2 is not a constant in general but a function of A. We expand λ_2 by the power series of A as

$$\lambda_2 = \lambda_{20} + \lambda_{21}A + \lambda_{22}A^2 + \ldots$$

The first term λ_{20} is relevant to the saddle-node bifurcation, i.e., the breaking of reflectional symmetry.

We did not consider here the correction of A due to the nonlinear coupling between Ψ and ω. The amplitude A must be corrected as $A + \delta A$ where δA may be determined solely by the Reynolds number. This δA correction may also causes the symmetry breaking discussed here. It is difficult, however, to determine the correction δA analytically in general.

To illustrate how the azimuthal shear flow breaks the symmetry, we study here the simplest case when the azimuthal flow is approximated by the Stokes' solution

which is given by Eq.(6). In this case, since the amplitude of the Stokes' flow can be determined independently of the Rayleigh number and the amplitude of the convection, λ_2 is expressed only by the first term λ_{20}. The azimuthal flow term is reduced to

$$N_1(\omega_{st}, \omega_{st}) = \frac{Re^2}{3}\left[\frac{Pr\,R}{(R+1)^3 - R^3}\right]\left[\frac{(R+1)^3}{r^5} - \frac{1}{r^2}\right]\tilde{P}_2(\cos\vartheta). \qquad (20)$$

Since this term has a component of a Legendre polynomial $P_l(\cos\vartheta)$ of $l = 2$, we will study the case when the critical (neutral) mode of the linear stability of the trivial solution is given by $l = 2$. (Remember that the system has the spherical symmetry when the differential rotation is absent so that the critical mode $\tilde{\mathbf{X}}$ of the linear stability problem must be expressed by a Legendre function $P_l(\cos\vartheta)$ with a fixed l, i.e.,

$$\tilde{\mathbf{X}} \propto {}^t(\Psi_l(r)\tilde{P}_l(\cos\vartheta), T_l(r)P_l(\cos\vartheta)) \qquad (21)$$

where Ψ_l, T_l are the functions of r. Thus the function subspaces on which whole dynamics are projected are labeled by the order of Legendre polynomial l.)

The equilibrium amplitudes of perturbative analysis are compared with the numerical solution for the case of $R = 0.5$ and $6700 < Ra < 6900$ in Fig.5 ($Re = 0$) and in Fig.6 ($Re = 0.1$). Solid lines denote the value of u_0 for the numerical solutions. Dotted ones, on the other hand, denote the value of u_0 computed by extracting only the $l = 2$ mode from the numerical solutions, i.e., the amplitude of the solutions projected on $l = 2$ subspace. Broken ones are the amplitude calculated from the perturbative analysis of Eqs.(17) and (18). The coincidence of the amplitudes of the numerical solution and the weakly nonlinear amplitude equation is very well around the bifurcation point.

5 Summary and discussion

We investigated the effect of the differential rotation of the inner sphere on the thermal convection in a spherical shell. Differential rotation is thought to be the simplest way to create an azimuthal shear flow to the fluid between the concentric spheres. Axisymmetric steady solutions are obtained numerically by the Newton-Raphson's iterative method and their linear stability to axisymmetric disturbances is analyzed.

It is found that the pitchfork bifurcation, which occurs when the differential rotation is absent, is structurally unstable and becomes imperfect when the differential rotation is present. The solution branches of the perfect pitchfork bifurcation splits into two parts: one is a smooth transition from the 2-roll to the upward solution, and the other is a saddle-node bifurcation to the 2-roll solution and the downward solution. It is quite interesting that this splitting occurs not only on the most unstable branches but on all the symmetric solution branches.

The intrinsic symmetries of the system are discussed and it is found that the relevant symmetry that assures the pitchfork bifurcation is different between the symmetric solution case and the antisymmetric one. The cause of the imperfect bifurcation of the *symmetric* solution is the breaking of the asymptotic reflectional symmetry by the weak shear flow where the symmetry is a consequence of the self-adjointness of the linearized system. Weakly nonlinear analysis is carried out and the result is compared with the numerically obtained solution for the case when the shear flow is approximated by the Stokes' solution.

We comment the reason why we restricted our study to the axisymmetric case and the relation of our study to the non-axisymmetric stability problem. For $Re > 0$ the trivial solution no longer exists. Differential rotation yields the meridional circulation (spherical Couette flow) whose analytical expression has not been found yet. It is obvious that non-axisymmetric bifurcation must stem from the

solution branch obtained here. The present study illustrates the multiplicity of the axisymmetric solution at assigned parameters and their complex and interesting bifurcation features. Thus we regard our present work as the inevitable first step to the more general, non-axisymmetric stability problem.

It is well known that a non-axisymmetric (sectoral) disturbance gives the critical Rayleigh number for the thermal instability in a spherical shell with solid-body rotation. In the present problem, on the other hand, there are two reasons which make it plausible that an axisymmetric (zonal) mode is the most unstable.

The thermal convection problem with sheared flow between the horizontal parallel plates has been investigated by many authors. Deardorff[13] found that the critical Rayleigh number is given by a longitudinal roll whose axis is parallel to the direction of the shear flow. The transversal rolls whose axis is not parallel to the direction of the shear flow is stabilized in the presence of the shear flow. This result suggests that an axisymmetric (zonal) disturbance gives the marginal mode and non-axisymmetric (tesseral) disturbances are stabilized under the effect of the differential rotation.

When the differential rotation is present, the yielded spherical Couette flow intrinsically has finite amplitude zonal components of even l's. Thus, one can expect that one of these components is amplified by the buoyancy effect more easily than tesseral modes which is not contained in the spherical Couette flow.

The stability against non-axisymmetric disturbances is our next concern. It is of our interest what kind of bifurcation occurs. It is well known that, when the differential rotation is absent, the neutrally stable modes are degenerated due to the spherical symmetry. How this degeneracy is removed and what is the role of the differential rotation? The investigation of this problem is under way.

Acknowledgments

The authors express their cordial thanks to Prof. H. Okamoto and Dr. S. Toh for valuable discussions. We also give our gratitude to Prof. S. Kida for his critical comments on the manuscript and to Prof. K. Fujimura for valuable advises. This work was partially supported by a Grant-in-Aid from the Ministry of Education, Science and Culture.

References

[1] S. Chandrasekhar, *Hydrodynamic and hydromagnetic stability*, (Oxford Univ. Press, London,1961), Chapt.VI.

[2] F. H. Busse, "Patterns of convection in spherical shells," J. Fluid Mech. **72**, 67 (1975).

[3] M. Golubitsky, I. Stewart, and D. G. Schaeffer, *Singularities and groups in bifurcation theory, Vol. II*, (Springer-Verlag, New York, 1988).

[4] J. D. Rodriguez, C. Geiger, and G. Dangelmayr, "Codimension two local analysis of spherical Bénard convection," in *Dynamics, Bifurcation and Symmetry*, edited by P. Chossat (Kluwer, the Netherlands, 1994), pp.279-289.

[5] P. Chossat, and F. Guyard, "A classification of 2-modes interactions with $SO(3)$ symmetry and applications," in *Dynamics, Bifurcation and Symmetry* edited by P. Chossat (Kluwer, the Netherlands, 1994), pp.79-95.

[6] P. S. Marcus, and L. S. Tuckerman, "Simulation of flow between concentric rotating spheres. Part 1, Steady states," J. Fluid Mech. **185**, 1 (1987).

[7] P. S. Marcus, and L. S. Tuckerman, "Simulation of flow between concentric rotating spheres. Part 2, Transitions," J. Fluid Mech. **185**, 31 (1987).

[8] K. Büler, "Symmetric and asymmetric Taylor vortex flow in spherical gaps," Acta Mechanica **81**, 3 (1990).

[9] Y. N. Belyaev, A. A. Monakhov, and I. M. Yavorskaya, "Stability of spherical Couette flow in thick layers when the inner sphere revolves," Fluid Dyn. **13**, 162 (1978), [Transl. Izv. AN SSSR. Meh. Zhidkhosti i Gaza **2**, 9-15].

[10] C. K. Mamun, and L. S. Tuckerman, "Asymmetry and Hopf bifurcation in spherical Couette flow," Phys. Fluids **7**, 80 (1995).

[11] K. Araki, S. Yanase, and J. Mizushima, "Bifurcation in a flow between two concentric spheres with different temperatures," in *Unstable and turbulent motion of fluid*, edited by S. Kida (World Scientific, Singapore, 1993) pp.59-70.

[12] S. Yanase, J. Mizushima, and K. Araki, "Multiple solutions for a flow between two concentric spheres with different temperatures and their stability," J. Phys. Soc. Japan **64**, 2433 (1995).

[13] J. W. Deardorff, "Gravitational instability between horizontal plates with shear," Phys. Fluids **8**, 1027 (1965).

[14] K. Araki, J. Mizushima, and S. Yanase, "Thermal instability of a fluid in a spherical shell with thin layer approximation analysis," J. Phys. Soc. Jpn. **63**, 2123(1994).

[15] D. D. Joseph, and S. Carmi, "Subcritical convective instability. Part 2. Spherical shells," J. Fluid Mech. **26**, 769 (1966).

Appendix

In the Appendix, the weakly nonlinear analysis of the bifurcation of the symmetric solution for $Re = 0$ is reviewed. We will show in the course of the derivation of the amplitude equation that the system for $Re = 0$ has an asymptotic reflectional symmetry and that the self-adjointness of linear problem is relevant to this symmetry rather than the geometry of the system. It should be remarked that the content of this section is somewhat a paraphrase of the result of Joseph and Carmi[15].

Following the usual procedure, we take $Ra - Rac$ as a bifurcation parameter and expand the variables in powers of $\epsilon = \sqrt{Ra - Rac}$. The Rayleigh number, time, stream functions and temperature fluctuation are expanded as follows:

$$Ra = Ra_c + \epsilon^2, \tag{22a}$$

$$t = \epsilon^2 t_2 + \epsilon^3 t_3 + o(\epsilon^3). \tag{22b}$$

$$\Psi = \epsilon\Psi_1 + \epsilon^2\Psi_2 + \epsilon^3\Psi_3 + o(\epsilon^3), \tag{22c}$$

$$\omega = \epsilon\omega_1 + \epsilon^2\omega_2 + \epsilon^3\omega_3 + o(\epsilon^3), \tag{22d}$$

$$T = \epsilon T_1 + \epsilon^2 T_2 + \epsilon^3 T_3 + o(\epsilon^3), \tag{22e}$$

Substituting Eqs.(22) into the basic equations (3a)-(3c), we obtain at $O(\epsilon)$

$$L_0 \mathbf{X}_1 = 0 \tag{23a}$$

$$D^2\omega_1 = 0 \tag{23b}$$

where

$$L_0 = \begin{pmatrix} Pr\, D^2 D^2 & Ra_c \sin\vartheta \left(\frac{R^2}{r^2}\right) \frac{\partial}{\partial\vartheta} \\ \frac{R(R+1)}{r^4 \sin\vartheta} \frac{\partial}{\partial\vartheta} & \triangle \end{pmatrix}, \quad X_i = \begin{pmatrix} \Psi_i \\ T_i \end{pmatrix} \quad (i = 1, 2, 3, ...). \tag{24}$$

Eq. (23b) has only a trivial solution, $\omega_1 = 0$. On the other hand, Eq. (23a) has a non-trivial solution $\mathbf{X}_1$ at the critical Rayleigh number Ra_c under the boundary

conditions (1a) and (1b). To solve Eq. (23a) the collocation method with the expansions (8a)-(8c) is adopted. The eigenvalue problem is solved using the double QR algorithm.

At $O(\epsilon^2)$, we have

$$L_0 \mathbf{X}_2 = -N_{\mathbf{X}}(\mathbf{X}_1, \mathbf{X}_1), \tag{25a}$$

$$D^2 \omega_2 = 0, \tag{25b}$$

where

$$N_{\mathbf{X}}(\mathbf{X}_i, \mathbf{X}_j) = {}^t(N_2(\Psi_i, \Psi_j), J(\Psi_i, T_j)). \tag{26}$$

The equation for ω_2 also has only a trivial solution. In order to obtain the solvability condition for the inhomogeneous equation for $\mathbf{X}_2$, we introduce the following inner product:

$$\langle \mathbf{X}_A, \mathbf{X}_B \rangle = -\iiint \Psi_A \Psi_B \frac{\mathrm{d}r\mathrm{d}\vartheta\mathrm{d}\varphi}{\sin\vartheta} + \frac{Pr\, Ra_c\, R}{R+1} \iiint T_A T_B r^2 \sin\vartheta \mathrm{d}r\mathrm{d}\vartheta\mathrm{d}\varphi, \tag{27}$$

for any $\mathbf{X}_A = {}^t(\Psi_A, T_A)$ and $\mathbf{X}_B = {}^t(\Psi_B, T_B)$, and the integrations are carried out on the whole spherical shell. This inner product yields the relation that $L^\dagger = L_0$ where $L^\dagger$ is the adjoint operator of L_0. This condition is slightly stronger than the self-adjointness which is usually found in many literatures. The solvability condition for $\mathbf{X}_2$ is that r.h.s. of the equation has no projection on the kernel of the linear operator L_0, i.e.,

$$\left\langle \mathbf{X}^\dagger, N_{\mathbf{X}}(\mathbf{X}_1, \mathbf{X}_1) \right\rangle = 0. \tag{28}$$

Because the linear operator L_0 is self-adjoint, i.e., $\mathbf{X}^\dagger = C\mathbf{X}_1$ where C is an arbitrary constant and because $\mathbf{X}_1 = \mathbf{0}$ at the boundaries, this condition(28) is exactly satisfied. Thus the equation for $\mathbf{X}_2$ can be solved as

$$\mathbf{X}_2 = -(L_0)^{-1} N_{\mathbf{X}}(\mathbf{X}_1, \mathbf{X}_1), \tag{29}$$

where $(L_0)^{-1}$ denotes the inverse operator of L_0. Singular value decomposition algorithm is used to solve this equation numerically.

At $O(\epsilon^3)$, we obtain the the equation

$$L_0 \mathbf{X}_3 = \frac{\partial}{\partial t_2} M\mathbf{X}_1 - (Ra - Ra_c)L_2\mathbf{X}_1 - N_{\mathbf{X}}(\mathbf{X}_2, \mathbf{X}_1) - N_{\mathbf{X}}(\mathbf{X}_1, \mathbf{X}_2), \quad (30a)$$

$$D^2\omega_3 = 0, \quad (30b)$$

where

$$M = \begin{pmatrix} D^2 & 0 \\ 0 & \mathbf{1} \end{pmatrix}, \quad L_2 = \begin{pmatrix} 0 & \sin\vartheta\gamma(r)\dfrac{\partial}{\partial\vartheta} \\ 0 & 0 \end{pmatrix}. \quad (31)$$

The equation for ω_3 has only a trivial solution. The solvability condition for the inhomogeneous equation for $\mathbf{X}_3$ leads to

$$\begin{aligned} &\frac{\partial}{\partial t_2}\left\langle \mathbf{X}^\dagger, M\mathbf{X}_1 \right\rangle - (Ra - Ra_c)\left\langle \mathbf{X}^\dagger, L_2\mathbf{X}_1 \right\rangle \\ &\quad - \left\langle \mathbf{X}^\dagger, N_{\mathbf{X}}(\mathbf{X}_2, \mathbf{X}_1) + N_{\mathbf{X}}(\mathbf{X}_1, \mathbf{X}_2) \right\rangle = 0. \end{aligned} \quad (32)$$

Now we assume the $\mathbf{X}_1$ is separated as

$$\mathbf{X}_1 = A(t_2)\,\tilde{\mathbf{X}}(r, \vartheta), \quad (33)$$

where A is a real variable and $\tilde{\mathbf{X}}$ is a vector in $\mathrm{Ker}(L_0)$.

Substituting (33) into (32), we obtain the amplitude equation

$$\frac{\mathrm{d}A}{\mathrm{d}t_2} = (Ra - Ra_c)\lambda_0 A + \lambda_1 A^3. \quad (34)$$

The coefficients λ_0 and λ_1 are given by

$$\lambda_0 = \frac{\left\langle \tilde{\mathbf{X}}, L_2\tilde{\mathbf{X}} \right\rangle}{\left\langle \tilde{\mathbf{X}}, M\tilde{\mathbf{X}} \right\rangle}, \qquad \lambda_1 = \frac{\left\langle \tilde{\mathbf{X}}, N_{\mathbf{X}}(\tilde{\mathbf{X}}_2, \tilde{\mathbf{X}}) + N_{\mathbf{X}}(\tilde{\mathbf{X}}, \tilde{\mathbf{X}}_2) \right\rangle}{\left\langle \tilde{\mathbf{X}}, M\tilde{\mathbf{X}} \right\rangle}, \quad (35)$$

where we put $\mathbf{X}^\dagger = \tilde{\mathbf{X}}$ and $\tilde{\mathbf{X}}_2 = -(L_0)^{-1}N_{\mathbf{X}}(\tilde{\mathbf{X}}, \tilde{\mathbf{X}})$. Numerical integrations are carried out according to the Gauss-Chebyshev quadrature formula in r-direction and the Gauss-Legendre quadrature formula in ϑ-direction.

Figure captions

Fig.1. A sketch of configuration.

Fig.2. The Rayleigh number Ra dependence of the symmetric solutions for $Re = 0$: (a) u_0, the radial velocity u_r at $(r, \vartheta) = (R + 1/2, \pi/2)$, (b) $Nu - 1$. The used symbols are as follows: 8-roll solutions are denoted by circles ($\circ$), 10-roll solutions by squares ($\Box$) and 6-roll solutions by triangles ($\triangle$). The upward solutions are denoted by open symbols and the downward ones by solid symbols. The contours for the meridional stream functions $\Psi(r, \vartheta)$ in the upper hemisphere for $Ra = 3000$ are also depicted in (b) with the abbreviated name of the solution. Only the upper hemisphere part of each stream function is depicted since the flow is symmetric with respect to the equator. The solid lines depict the clockwise circulations and the broken lines the anticlockwise circulations.

Fig.3. The Rayleigh number dependence of the symmetric solutions for $Re = 20$: (a) u_0, (b) $Nu - 1$. The symbols on the branches are consistently chosen with those in Fig.3. All the solutions with assigned symbols in this figure are obtained from those with the same symbols in Fig.3 ($Re = 0$) by changing the parameters Ra and Re adiabatically. The solution on the 2-roll branch bifurcated from the third saddle-node point is denoted by a cross symbol ($\times$). The contours for $\Psi(r, \vartheta)$ in the upper hemisphere for $Ra = 3000$ are also depicted in (b) with the abbreviated name of the solution.

Fig.4. A Schematic diagram of the bifurcations of a symmetric solution and an asymmetric solution. The vertical direction represents the antisymmetric subspace H_A. The horizontal directions represent the symmetric subspace H_S and the bifurcation parameter Ra. Because the equatorial reflection operator Γ reverses the sign of the antisymmetric component of the asymmetric

solution, the symmetry guarantees the pitchfork bifurcation of the asymmetric solutions (X_1 and X_2) bifurcated from a symmetric solution (X_0). All the points in the symmetric subspace (hatched plane in the figure) are, on the other hand, the fixed points of the operator Γ. Therefore the pitchfork bifurcation of the symmetric solution is not guaranteed by this symmetry.

Fig.5. The Rayleigh number Ra dependence of u_0 for $R = 0.5$ and $Re = 0$. Solid lines show u_0 of the numerical solutions. Dotted ones, on the other hand, denote the value of u_0 computed by extracting only the $l = 2$ mode from the numerical solutions. Broken lines are u_0 calculated from the amplitude equation (17).

Fig.6. The Rayleigh number dependence of u_0 of the symmetric solutions for $R = 0.5$ and $Re = 20$. Solid lines and dotted lines are same as those in Fig.5. Broken lines are u_0 calculated from the amplitude equation (18).

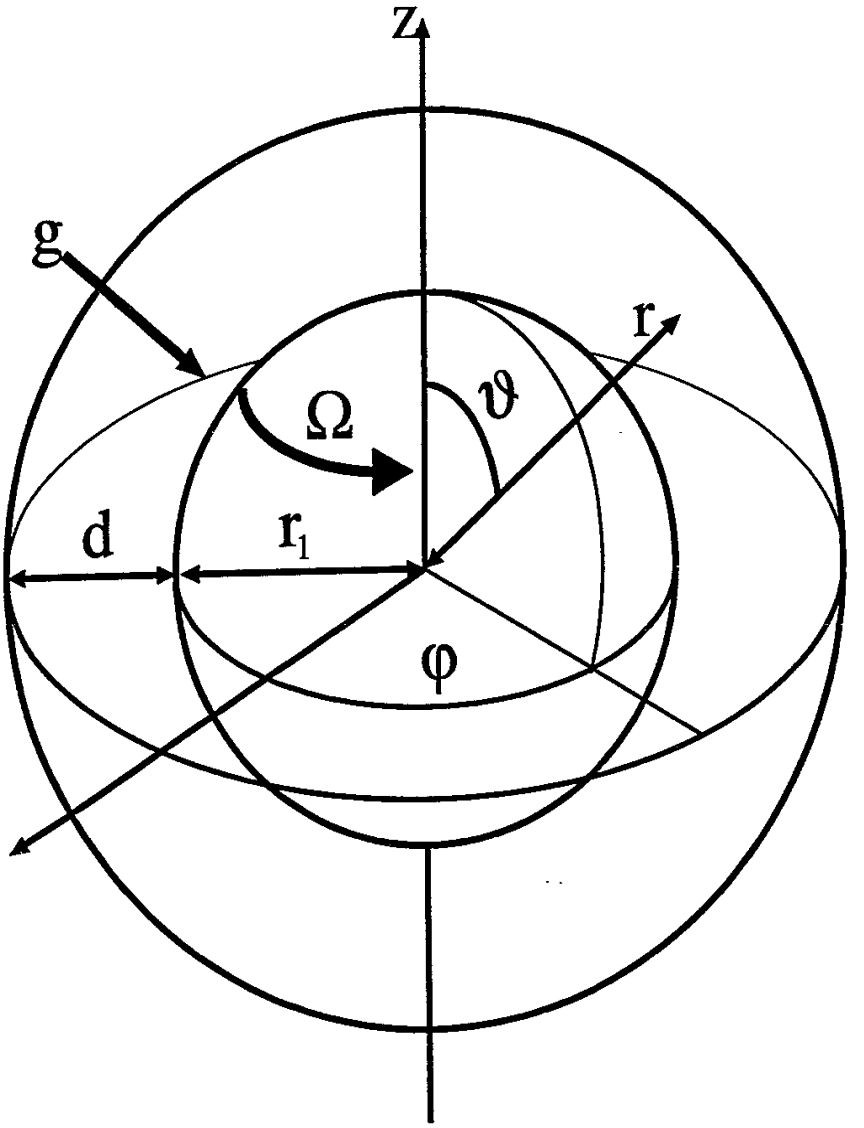

Fig. 1

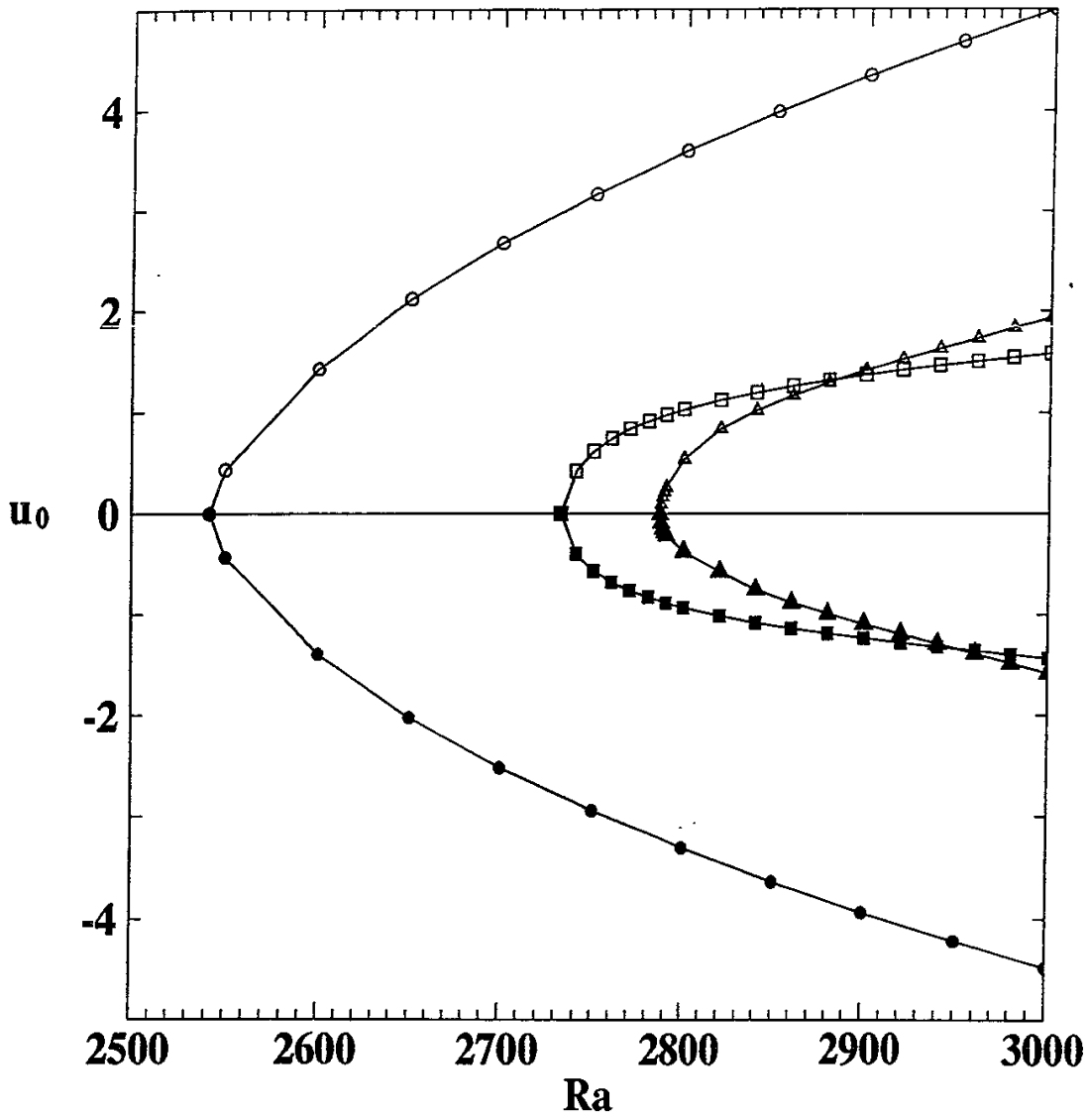

Fig. 2(a)

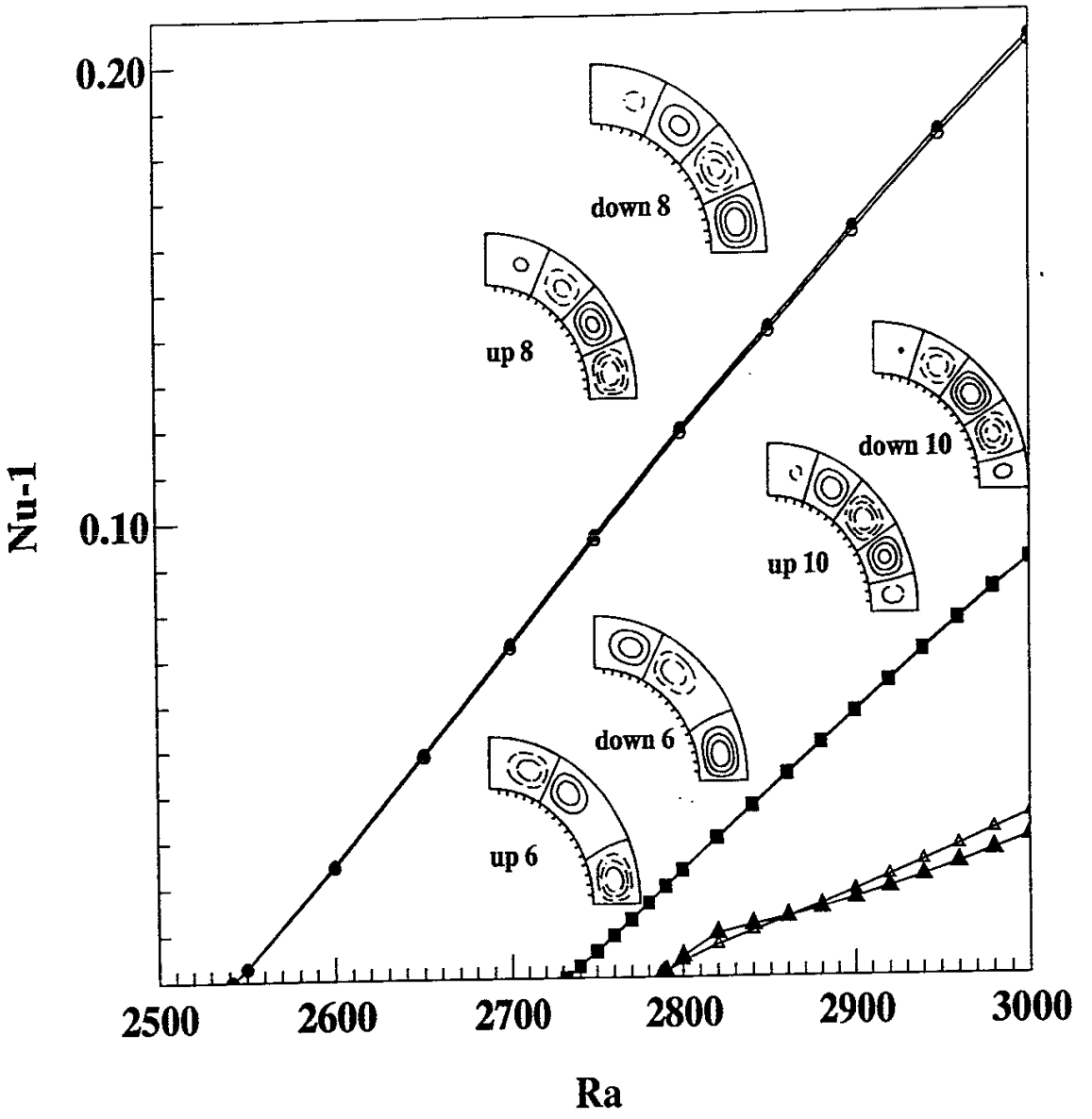
0.20
0.10
Nu-1
down 8
up 8
down 10
up 10
down 6
up 6
2500
2600
2700
2800
2900
3000
Ra

Fig. 2(b)

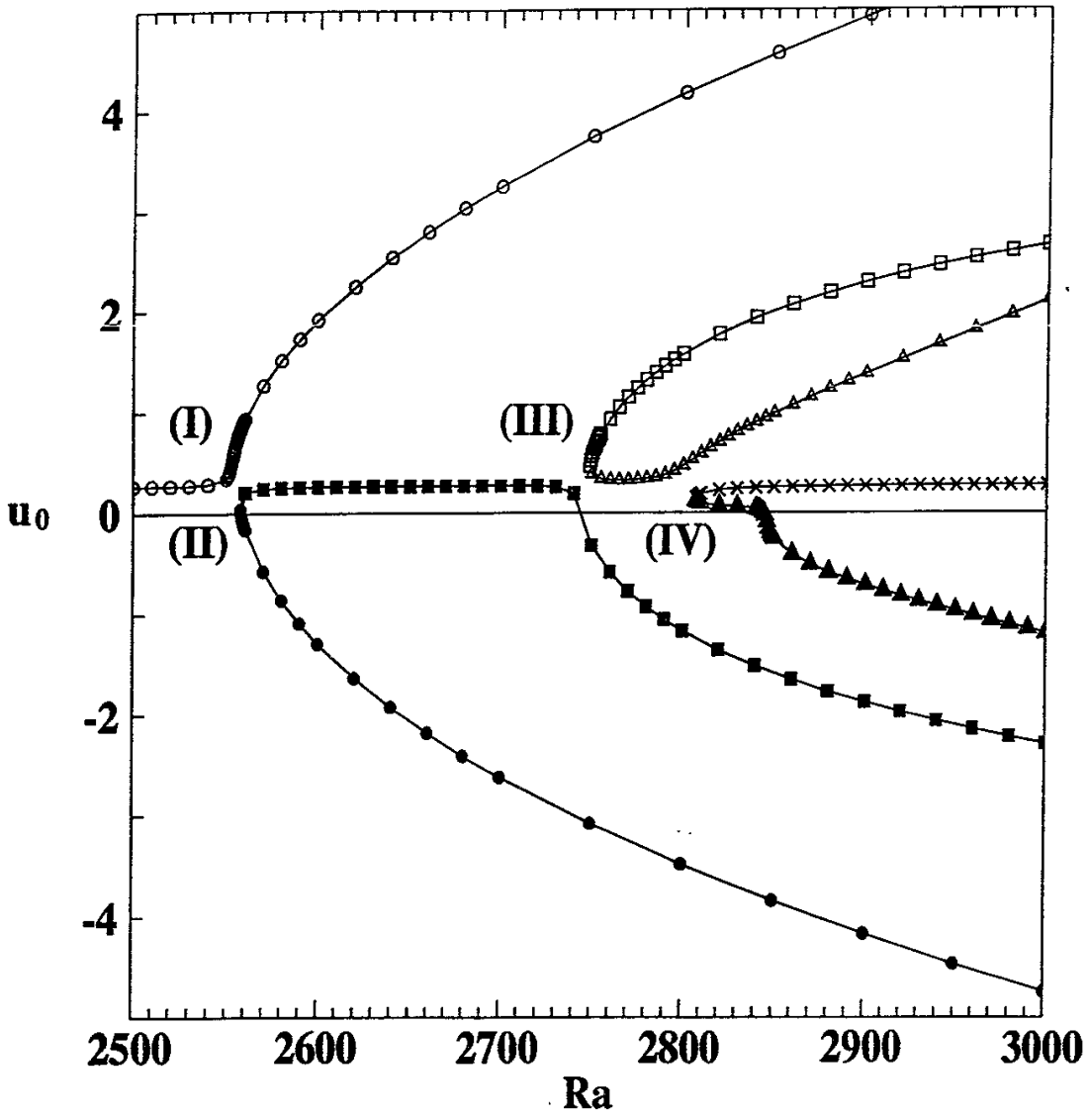

Fig. 3(a)

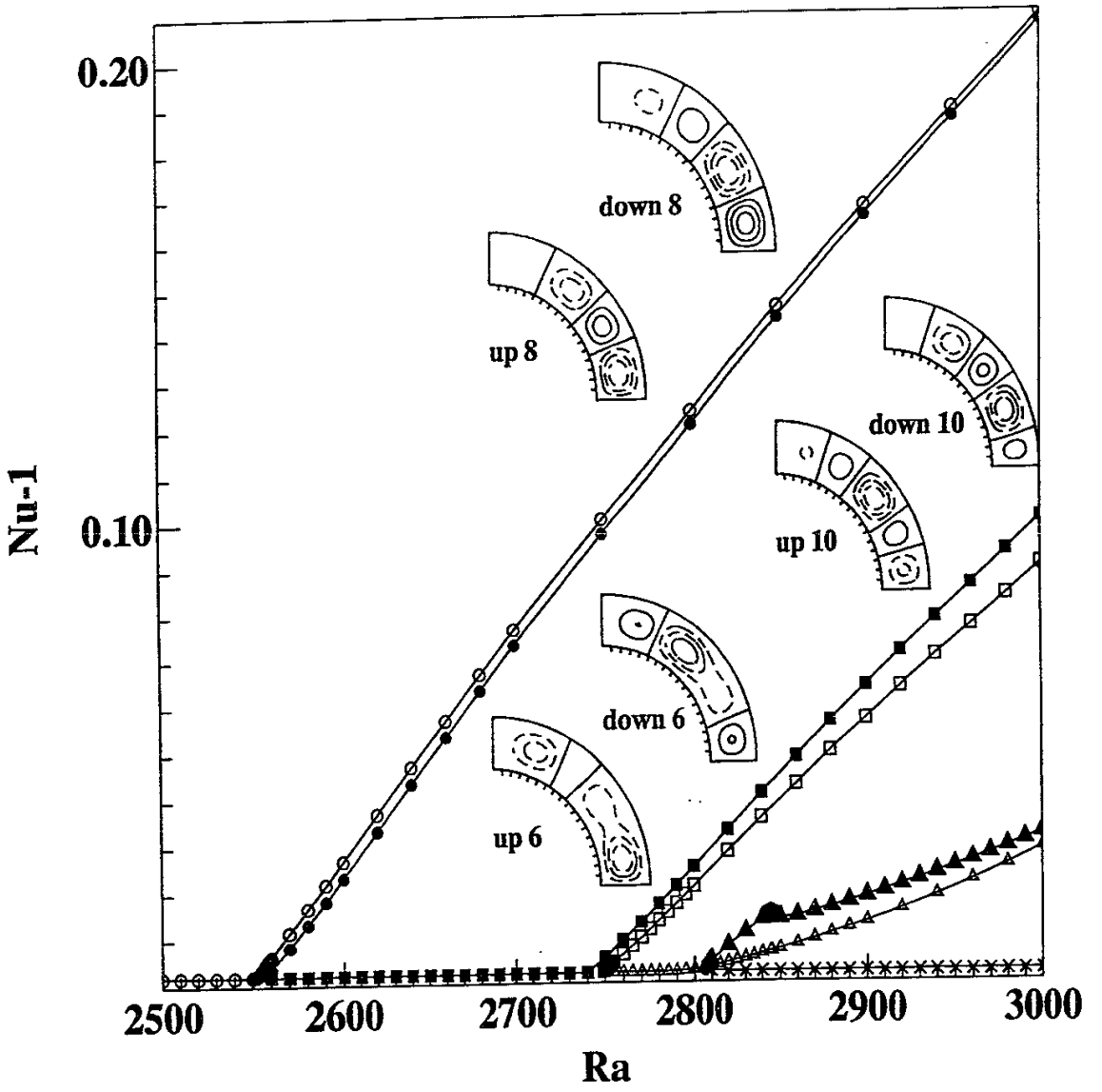
0.20
0.10
Nu-1
down 8
up 8
down 10
up 10
down 6
up 6
2500
2600
2700
2800
2900
3000
Ra

Fig. 3(b)

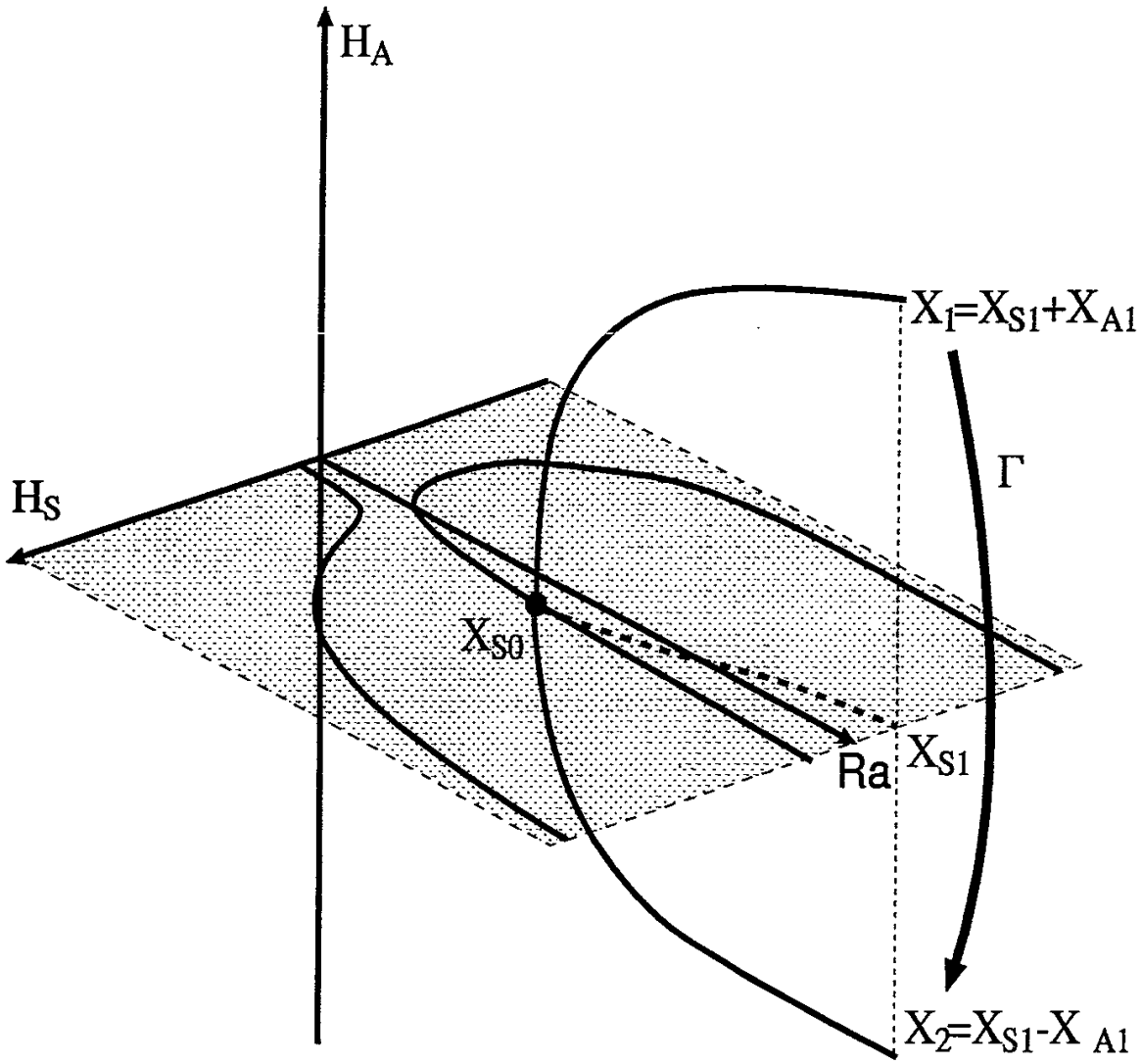

Fig. 4

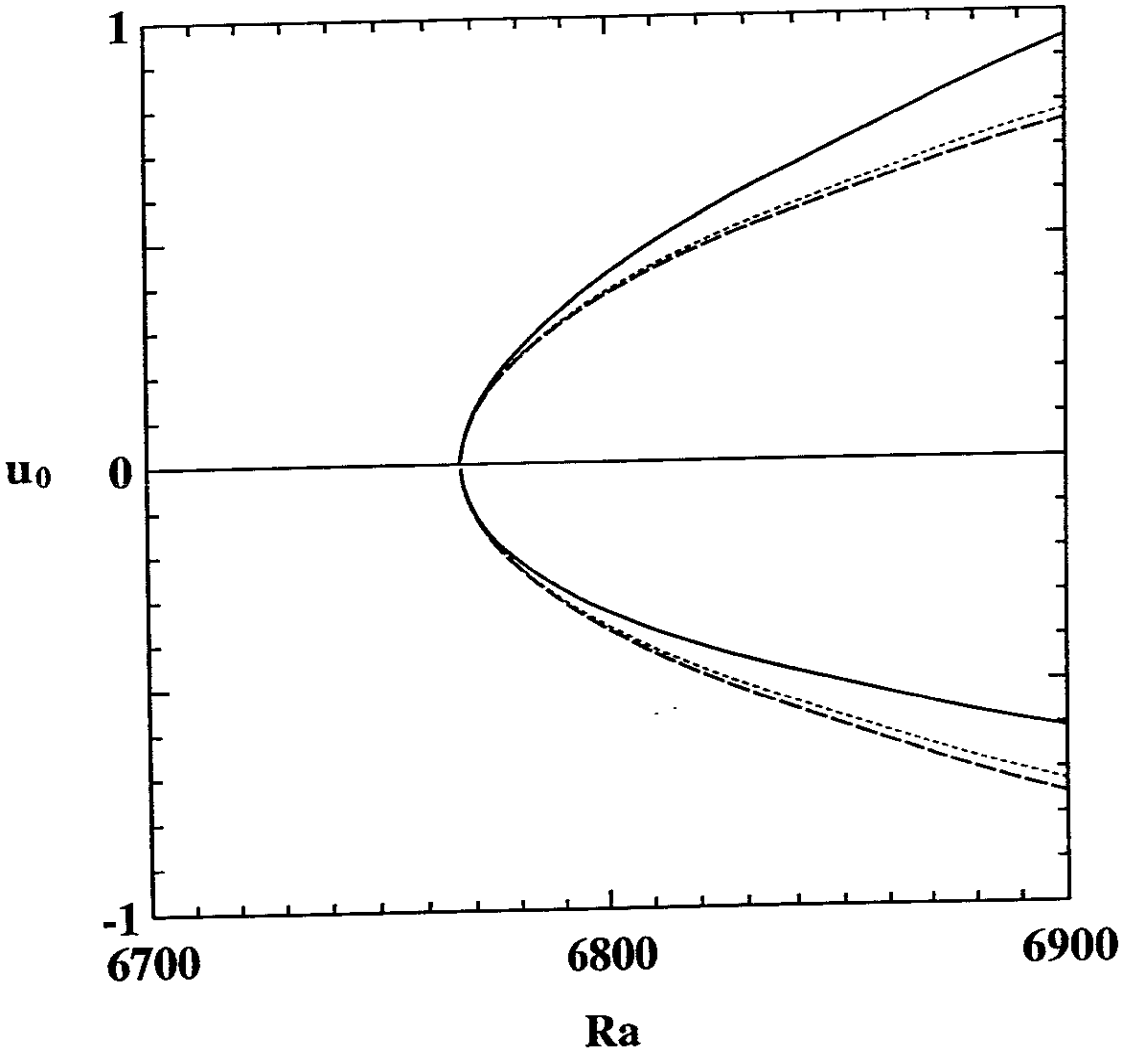

Fig. 5

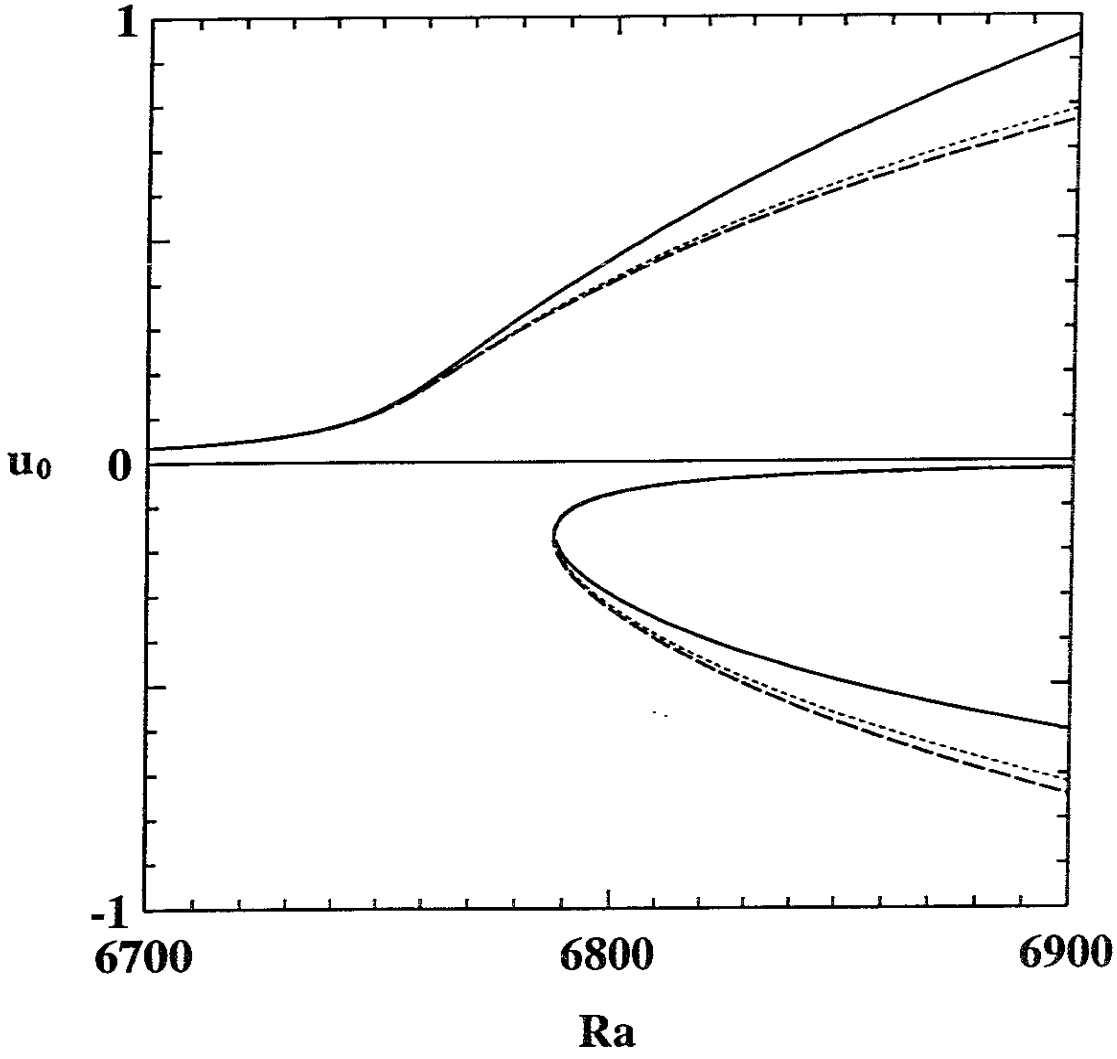

Fig. 6

Recent Issues of NIFS Series

NIFS-339 K. Toi, T. Morisaki, S. Sakakibara, S. Ohdachi, T.Minami, S. Morita, H. Yamada, K. Tanaka, K. Ida, S. Okamura, A. Ejiri, H. Iguchi, K. Nishimura, K. Matsuoka, A. Ando, J. Xu, I. Yamada, K. Narihara, R. Akiyama, H. Idei, S. Kubo, T. Ozaki, C. Takahashi, K. Tsumori, *H-Mode Study in CHS*; Feb. 1995

NIFS-340 T. Okada and H. Tazawa, *Filamentation Instability in a Light Ion Beam-plasma System with External Magnetic Field*; Feb. 1995

NIFS-341 T. Watanbe, G. Gnudi, *A New Algorithm for Differential-Algebraic Equations Based on HIDM*; Feb. 13, 1995

NIFS-342 Y. Nejoh, *New Stationary Solutions of the Nonlinear Drift Wave Equation;* Feb. 1995

NIFS-343 A. Ejiri, S. Sakakibara and K. Kawahata, *Signal Based Mixing Analysis for the Magnetohydrodynamic Mode Reconstruction from Homodyne Microwave Reflectometry*; Mar.. 1995

NIFS-344 B.B.Kadomtsev, K. Itoh, S.-I. Itoh *Fast Change in Core Transport after L-H Transition*; Mar. 1995

NIFS-345 W.X. Wang, M. Okamoto, N. Nakajima and S. Murakami, *An Accurate Nonlinear Monte Carlo Collision Operator*; Mar. 1995

NIFS-346 S. Sasaki, S. Takamura, S. Masuzaki, S. Watanabe, T. Kato, K. Kadota, *Helium I Line Intensity Ratios in a Plasma for the Diagnostics of Fusion Edge Plasmas*; Mar. 1995

NIFS-347 M. Osakabe, *Measurement of Neutron Energy on D-T Fusion Plasma Experiments;* Apr. 1995

NIFS-348 M. Sita Janaki, M.R. Gupta and Brahmananda Dasgupta, *Adiabatic Electron Acceleration in a Cnoidal Wave;* Apr. 1995

NIFS-349 J. Xu, K. Ida and J. Fujita, *A Note for Pitch Angle Measurement of Magnetic Field in a Toroidal Plasma Using Motional Stark Effect*; Apr. 1995

NIFS-350 J. Uramoto, *Characteristics for Metal Plate Penetration of a Low Energy Negative Muonlike or Pionlike Particle Beam*: Apr. 1995

NIFS-351 J. Uramoto,
An Estimation of Life Time for A Low Energy Negative Pionlike Particle Beam: Apr. 1995

NIFS-352 A. Taniike,
Energy Loss Mechanism of a Gold Ion Beam on a Tandem Acceleration System: May 1995

NIFS-353 A. Nishizawa, Y. Hamada, Y. Kawasumi and H. Iguchi,
Increase of Lifetime of Thallium Zeolite Ion Source for Single-Ended Accelerator: May 1995

NIFS-354 S. Murakami, N. Nakajima, S. Okamura and M. Okamoto,
Orbital Aspects of Reachable β Value in NBI Heated Heliotron/Torsatrons; May 1995

NIFS-355 H. Sugama and W. Horton,
Neoclassical and Anomalous Transport in Axisymmetric Toroidal Plasmas with Electrostatic Turbulence; May 1995

NIFS-356 N. Ohyabu
A New Boundary Control Scheme for Simultaneous Achievement of H-mode and Radiative Cooling (SHC Boundary); May 1995

NIFS-357 Y. Hamada, K.N. Sato, H. Sakakita, A. Nishizawa, Y. Kawasumi, R. Liang, K. Kawahata, A. Ejiri, K. Toi, K. Narihara, K. Sato, T. Seki, H. Iguchi, A. Fujisawa, K. Adachi, S. Hidekuma, S. Hirokura, K. Ida, M. Kojima, J. Koong, R. Kumazawa, H. Kuramoto, T. Minami,. M. Sasao, T. Tsuzuki, J.Xu, I. Yamada, and T. Watari,
Large Potential Change Induced by Pellet Injection in JIPP T-IIU Tokamak Plasmas; May 1995

NIFS-358 M. Ida and T. Yabe,
Implicit CIP (Cubic-Interpolated Propagation) Method in One Dimension; May 1995

NIFS-359 A. Kageyama, T. Sato and The Complexity Simulation Group,
Computer Has Solved A Historical Puzzle: Generation of Earth's Dipole Field; June 1995

NIFS-360 K. Itoh, S.-I. Itoh, M. Yagi and A. Fukuyama,
Dynamic Structure in Self-Sustained Turbulence; June 1995

NIFS-361 K. Kamada, H. Kinoshita and H. Takahashi,
Anomalous Heat Evolution of Deuteron Implanted Al on Electron Bombardment; June 1995

NIFS-362 V.D. Pustovitov,

Suppression of Pfirsch-schlüter Current by Vertical Magnetic Field in Stellarators; June 1995

NIFS-363 A. Ida, H. Sanuki and J. Todoroki
An Extended K-dV Equation for Nonlinear Magnetosonic Wave in a Multi-Ion Plasma; June 1995

NIFS-364 H. Sugama and W. Horton
Entropy Production and Onsager Symmetry in Neoclassical Transport Processes of Toroidal Plasmas; July 1995

NIFS-365 K. Itoh, S.-I. Itoh, A. Fukuyama and M. Yagi,
On the Minimum Circulating Power of Steady State Tokamaks; July 1995

NIFS-366 K. Itoh and Sanae-I. Itoh,
The Role of Electric Field in Confinement; July 1995

NIFS-367 F. Xiao and T. Yabe,
A Rational Function Based Scheme for Solving Advection Equation; July 1995

NIFS-368 Y. Takeiri, O. Kaneko, Y. Oka, K. Tsumori, E. Asano, R. Akiyama, T. Kawamoto and T. Kuroda,
Multi-Beamlet Focusing of Intense Negative Ion Beams by Aperture Displacement Technique; Aug. 1995

NIFS-369 A. Ando, Y. Takeiri, O. Kaneko, Y. Oka, K. Tsumori, E. Asano, T. Kawamoto, R. Akiyama and T. Kuroda,
Experiments of an Intense H- Ion Beam Acceleration; Aug. 1995

NIFS-370 M. Sasao, A. Taniike, I. Nomura, M. Wada, H. Yamaoka and M. Sato,
Development of Diagnostic Beams for Alpha Particle Measurement on ITER; Aug. 1995

NIFS-371 S. Yamaguchi, J. Yamamoto and O. Motojima;
A New Cable -in conduit Conductor Magnet with Insulated Strands; Sep. 1995

NIFS-372 H. Miura,
Enstrophy Generation in a Shock-Dominated Turbulence; Sep. 1995

NIFS-373 M. Natsir, A. Sagara, K. Tsuzuki, B. Tsuchiya, Y. Hasegawa, O. Motojima,
Control of Discharge Conditions to Reduce Hydrogen Content in Low Z Films Produced with DC Glow; Sep. 1995

NIFS-374 K. Tsuzuki, M. Natsir, N. Inoue, A. Sagara, N. Noda, O. Motojima, T. Mochizuki, I. Fujita, T. Hino and T. Yamashina,
Behavior of Hydrogen Atoms in Boron Films during H_2 and He Glow

Discharge and Thermal Desorption; Sep. 1995

NIFS-375 U. Stroth, M. Murakami, R.A. Dory, H. Yamada, S. Okamura, F. Sano and T. Obiki,
Energy Confinement Scaling from the International Stellarator Database; Sep. 1995

NIFS-376 S. Bazdenkov, T. Sato, K. Watanabe and The Complexity Simulation Group,
Multi-Scale Semi-Ideal Magnetohydrodynamics of a Tokamak Plasma; Sep. 1995

NIFS-377 J. Uramoto,
Extraction of Negative Pionlike Particles from a H2 or D2 Gas Discharge Plasma in Magnetic Field; Sep. 1995

NIFS-378 K. Akaishi,
Theoretical Consideration for the Outgassing Characteristics of an Unbaked Vacuum System; Oct. 1995

NIFS-379 H. Shimazu, S. Machida and M. Tanaka,
Macro-Particle Simulation of Collisionless Parallel Shocks; Oct. 1995

NIFS-380 N. Kondo and Y. Kondoh,
Eigenfunction Spectrum Analysis for Self-organization in Dissipative Solitons; Oct. 1995

NIFS-381 Y. Kondoh, M. Yoshizawa, A. Nakano and T. Yabe,
Self-organization of Two-dimensional Incompressible Viscous Flow in a Friction-free Box; Oct. 1995

NIFS-382 Y.N. Nejoh and H. Sanuki,
The Effects of the Beam and Ion Temperatures on Ion-Acoustic Waves in an Electron Beam-Plasma System; Oct. 1995

NIFS-383 K. Ichiguchi, O. Motojima, K. Yamazaki, N. Nakajima and M. Okamoto
Flexibility of LHD Configuration with Multi-Layer Helical Coils; Nov. 1995

NIFS-384 D. Biskamp, E. Schwarz and J.F. Drake,
Two-dimensional Electron Magnetohydrodynamic Turbulence; Nov. 1995

NIFS-385 H. Kitabata, T. Hayashi, T. Sato and Complexity Simulation Group,
Impulsive Nature in Collisional Driven Reconnection; Nov. 1995

NIFS-386 Y. Katoh, T. Muroga, A. Kohyama, R.E. Stoller, C. Namba and O. Motojima,
Rate Theory Modeling of Defect Evolution under Cascade Damage Conditions:The Influence of Vacancy-type Cascade Remnants and Application to the Defect Production Chracterization by Microstructural Analysis; Nov. 1995